Stress anisotropy and wave propagation: a micromechanical view

J.C. Santamarina and G. Cascante

Abstract: Wave propagation is a constant-fabric macrophenomenon, suitable to microinterpretation. Both velocity and attenuation characterize state, including inherent and stress-induced anisotropy. The purpose of this research is to study the effect of isotropic and deviatoric stresses on wave propagation in particulate materials at low strains and to interpret results at the microlevel. A resonant-column device was modified to allow for the application of axial extension and axial compression deviatoric loading. The fixed-free boundary condition of the sample was maintained. Data for round, hard-grained sand show that shear wave velocity and attenuation are primarily dependent on the mean stress on the polarization plane, with minimal effect of the deviatoric component, in agreement with prior observations at stress ratios less than 2–3. Attenuation is strongly correlated with the mean stress in the polarization plane and the level of shear strain. Damping does not vanish at low strains, contrary to predictions based on hysteretic behavior; hence, other loss mechanisms must take place at low strains. Low-strain wave parameters are adequately corrected for mid-strain using modified hyperbolic models. Measured velocity and damping trends during isotropic and anisotropic loading qualitatively agree with predictions based on regular arrays.

Key words: mechanical waves, resonant column, damping, shear modulus, stress anisotropy, random vibration.

Résumé : La propagation d'ondes est un macro-phénomène à fabrique constante qui se prête à une micro-interprétation. Tant la vitesse que l'atténuation caractérisent l'état comprenant l'anisotropie inhérente et celle induite par les contraintes. Le but de la présente recherche est d'étudier l'effet des contraintes isotropes et déviatoriques sur la propagation d'ondes aux faibles déformations dans des matériaux constitués de particules, et d'interpréter les résultats à un micro-niveau. Un appareil à colonne résonnante a été modifié pour permettre l'application de chargements déviatoriques en extension et compression axiales. La condition de limite fixe-libre de l'échantillon a été maintenue. Les données pour le sable à grains durs arrondis montrent que la vitesse de l'onde de cisaillement et l'atténuation dépendent principalement de la contrainte moyenne sur le plan de polarisation, avec un effet minime de la composante déviatorique, en accord avec les observations antérieures faites à des rapports de contraintes inférieurs à 2–3. L'atténuation est fortement corrélée avec la contrainte moyenne dans le plan de polarisation et le niveau de déformation de cisaillement. L'amortissement ne disparaît pas aux faibles contraintes, contrairement aux prédictions basées sur le comportement en hystérèse; ainsi, d'autres mécanismes de perte doivent se produire aux faibles contraintes. Les paramètres d'ondes aux faibles déformations sont corrigés adéquatement pour les déformations moyennes en utilisant des modèles hyperboliques modifiés. La vitesse mesurée et les tendances à l'amortissement durant un chargement isotrope et anisotrope concordent qualitativement avec les prédictions basées sur les allures régulières.

Mots clés : ondes mécaniques, colonne résonnante, amortissement, module de cisaillement, anisotropie de contrainte, vibration aléatoire.

[Traduit par la rédaction]

Introduction

The propagation of low-strain mechanical waves is a small perturbation phenomenon that assesses the state of the soil without altering the fabric or causing permanent effects. Therefore, velocity and attenuation are constant-fabric characteristics of a soil and can be uniquely used to monitor ongoing internal changes in the medium.

Received September 14, 1995. Accepted June 24, 1996.

J.C. Santamarina. Georgia Institute of Technology, Atlanta, GA 30332-0355, U.S.A.
G. Cascante. University of Waterloo, Waterloo, ON N2L 3G1, Canada.

The state of a particulate medium can be described at the micromechanical level by characterizing the distribution of contacts, interparticle forces, and particle orientations. Therefore, it is theoretically feasible to relate the micromechanical characteristics of the particulate medium to the macrocharacteristics of wave propagation, i.e., velocity and attenuation and their frequency dependency. Empirical relations have been proposed. For example, there are first-order correlations between velocity and the state of stress, which include adequate corrections for void ratio. On the other hand, empirical relations for attenuation are scarce, even though it appears that attenuation is a clear indicator of geoprocesses such as loading, diagenesis, creep, cementation, and decementation.

The purpose of this study is to assess the effect of isotropic and deviatoric stresses on low-strain wave propagation in particulate materials. The resonant-column device and measurement procedure was modified to determine velocity and attenuation in samples subjected to axial compression and axial extension loading. Empirical relations and observed experimental results are analyzed with a micromechanics perspective.

The micromechanics of low-strain parameters

The stress-dependent deformation and strength behavior of soils follows from their particulate nature. In addition, the analysis of particle-to-particle interaction with contact theories such as Hertz and Mindlin explains the inherently nonlinear and nonelastic nature of soils. Such micromechanical analyses can be analytically or numerically used to study soils and to extend experimental observations.

The micromechanical representation involves particle orientations, contacts, and interaction forces among particles. The physical and geometrical properties of particles and their relative arrangement influence the macrobehaviour. Regular and isotropic random packings of monosized spheres have been extensively studied, in part because of their relative simplicity. Real soils can be analyzed as combinations of regular packings, matching properties such as porosity, density, and coordination number (Petrakis and Dobry 1987; Deresiewicz 1973).

Interparticle forces depend on the applied stresses and the degree of effective connections among particles, i.e., coordination number C_n. The minimum coordination number for stable configurations can be determined by equating the number of unknown forces and the number of equilibrium equations in the system. The coordination number most often observed in three-dimensional random packings is around $C_n = 8$, which is also the coordination number of the cubical-tetrahedral packing. The average coordination number has been related to the void ratio e by empirical equations, e.g.,

$$[1] \quad C_n = 13.28 - 8e \quad \text{(Chang et al. 1991)}$$

$$[2] \quad C_n = \frac{12}{1 + e} \quad \text{(Field 1963)}$$

$$[3] \quad C_n = 28.486 - 10.726(1 + e) \quad \text{(Smith et al. 1929)}$$

These regression equations hide substantial scatter. For example, significant changes in the coordination number may take place during conventional triaxial loading, even though the corresponding changes in void ratio can be relatively small (the coordination number can change from $C_n = 6.2$ to $C_n = 5$ while a dense sample subjected to deviatoric loading changes from initial contractive to dilative behavior $\Delta e \approx 0$; Chantawarangul 1993). Thus changes in void ratio may not reflect the real increase in coordination number. Particle eccentricity increases the average coordination number, affects the packing pattern, and decreases porosity (Fayed and Otten 1984; Aloufi and Santamarina 1995).

Numerical and experimental micromechanics research has shown that fabric anisotropy causes mechanical anisotropy. Conversely, stress anisotropy causes fabric and contact force anisotropy: the average number of contacts and the average normal contact force increase in the direction of the higher applied normal stress until limiting values of force and fabric anisotropy are reached. The polar distributions of micromechanical parameters can be approximated by a second- or fourth-order Fourier series. Using these approximations Rothenburg and Bathurst (1989) found that the macroscopic angle of internal shear strength is a function of the limiting anisotropy in contacts, and in tangential and normal forces.

When the wavelength is significantly longer than the internal scale of the material, such as particle size, propagation parameters can be defined for the equivalent continuum. The shear wave velocity V_s is

$$[4] \quad V_s = \sqrt{\frac{G}{\rho}}$$

where G is the shear modulus and ρ is the mass density of the medium. Damping D is defined as the ratio between the energy lost E_{loss} and the energy returned E_{return} by the system in each cycle:

$$[5] \quad D = \frac{1}{2\pi} \frac{E_{loss}}{E_{return}}$$

The velocity and attenuation in a given propagation mode can be computed from other propagation modes if Poisson's ratio ν is known (Fratta and Santamarina 1996). Poisson's ratio for isotropic-continuous media can be calculated knowing the ratio between the shear modulus G and the constrained modulus M, G/M:

$$[6] \quad \nu = \frac{2\left(\frac{G}{M}\right) - 1}{2\left(\frac{G}{M} - 1\right)}$$

Low- and high-strain Poisson's ratios reflect different deformation mechanisms in the particulate medium. The relationship between micromechanical parameters and constant fabric wave propagation parameters will be studied by assessing G, D, and ν.

Regular packings: isotropic loading

Expressions for the low-strain shear stiffness G of regular packings under isotropic loading are summarized in Table 1 (Petrakis and Dobry 1987; Wang and Nur 1992; and derivations by the authors as part of this study, Cascante 1996). Based on the hysteretic behavior of a Mindlin contact, the strain-dependent damping for a simple cubic packing D_1 can be computed from eq. 5 (Dobry et al. 1982):

$$[7] \quad D_1 = \frac{12}{5\pi}\left\{\frac{1 - \left(1 - \frac{\gamma}{\gamma_t}\right)^{5/2}}{\frac{\gamma}{\gamma_t}\left[1 - \left(1 - \frac{\gamma}{\gamma_t}\right)^{3/2}\right]} - \frac{5\left(2 - \frac{\gamma}{\gamma_t}\right)}{6\frac{\gamma}{\gamma_t}}\right\}$$

where the threshold strain γ_t is the strain between particles that causes global slippage at the contact

Table 1. Poisson's ratio ν and shear modulus G for isotropically loaded regular packings of monosize spheres.

Packing	Poisson's ratio ν_{pack}	Shear modulus G
Isotropic continuum	$\nu_{pack} = \nu$	$G_c = \rho V_s^2$
Simple cubic (SC) $C_n = 6$	$\nu_{pack} = 0$	$G_{SC} = \dfrac{\left[\frac{3}{2}(1-\nu)\sigma_o G^2\right]^{1/3}}{(2-\nu)}$
Body-centered cubic (BCC) $C_n = 8$	$\nu_{pack} = \dfrac{\nu}{2(3-2\nu)}$	$G_{BCC} = \dfrac{9\left[\frac{(1-\nu)}{6}\sigma_o G^2\right]^{1/3}}{(6-5\nu)}$
Face-centered cubic (FCC) $C_n = 12$	$\nu_{pack} = \dfrac{\nu}{8-5\nu}$	$G_{FCC} = \dfrac{(4-3\nu)\left[\frac{3\sigma_o G^2}{2(1-\nu)^2}\right]^{1/3}}{2(2-\nu)}$
Cubical tetrahedral (CT) (from S_{1212}) $C_n = 8$	$\nu_{pack} = \dfrac{(a+1)k^2-(a+2)k+1}{(3a-1)k^2+(a+2)k-1}$	$G_{CT} = \dfrac{3^{5/6}(4-3\nu)\left[\frac{3\sigma_o G^2}{2(1-\nu^2)}\right]^{1/3}}{5(2-\nu)}$
Cubical tetrahedral (CT) (from S_{1313}) $C_n = 8$	$k = \dfrac{2-\nu}{2(1-\nu)}$, $a = \sqrt[3]{128/3}$	$G_{CT} = \dfrac{2(1-\nu)\left[\frac{9\sigma_o G^2}{2(1-\nu^2)}\right]^{1/3}}{5(2-\nu)}$

Note: ν, G, Poisson's ratio and shear modulus of the material, respectively; σ_o, isotropic confinement; S_{ijkl}, elastic stiffness constant.

$$[8] \qquad \gamma_t = \frac{\left(\frac{9}{4}\right)^{1/3}(2-\nu)f\sigma_o^{2/3}}{(1-\nu)^{1/2}(1+\nu)^{1/6}G^{2/3}}$$

where f is the interparticle friction coefficient and σ_o is isotropic confinement. The evaluation of eq. 7 shows that damping depends on the confining pressure to an exponent $-2/3$ for a constant level of shear strain γ. Duffy and Mindlin (1957) computed the damping for the face-centered cubic array and also found a variation with confinement with exponent $-2/3$.

Equation 7 shows that attenuation depends on the strain level of the perturbation. Yet, it presumes constant fabric, thus it is applicable below the threshold strain, i.e., $\gamma < \gamma_t$. In real particulate materials, strains larger than the threshold strain produce changes in coordination number, alterations in the degree of particle frustration, and generalized particle rotation, which reduces energy losses. These processes justify the lower rate of increase in damping with strain observed in experimental studies, as compared with eq. 7.

Low-strain values for Poisson's ratio have been computed for different regular packings of monosized spheres. Equations are also summarized in Table 1. For a simple cubic packing $\nu_{pack} = 0$, since the stiffness matrix of the packing is diagonal, i.e., deformation localizes at contacts, with no lateral manifestation. Equations for Poisson's ratio are plotted in Fig. 1. Note that Poisson's ratio is low for small-strain phenomena. Most regular packings are anisotropic, and the standard relationship between Poisson's ratio and moduli (eq. 6) is not longer applicable.

Regular packings: anisotropic loading

Petrakis and Dobry (1987) used an incremental approach to derive expressions for the shear modulus of regular packings subjected to anisotropic loading at constant fabric. The shear modulus in a simple cubic (SC) array G_{sc} is governed by the stresses in the direction of particle motion σ_m and in the direction of wave propagation σ_p (Petrakis and Dobry 1987):

$$[9] \qquad G_{sc} = 2G^{2/3}\left(\frac{3(1-\nu)}{2(2-\nu)}\right)^{1/3}\left(\frac{\sigma_p\sigma_m}{\sigma_p+\sigma_m}\right)^{1/3}$$

The direction of propagation, principal stress directions, and packing directions are collinear. On the other hand, the shear modulus for a body-centered cubic packing G_{BCC} is determined by the mean effective stress (Petrakis and Dobry 1987):

$$[10] \qquad G_{BCC} = \frac{9G^{2/3}}{6-5\nu}\left(\frac{1-\nu}{6}\right)^{1/3}\left(\frac{\sigma_p+2\sigma_m}{3}\right)^{1/3}$$

The energy-based definition of damping (eq. 5) and Mindlin's contact permit deriving a relationship for damping in a simple cubic array subjected to anisotropic loading D_A (Cascante 1996). The resulting equation is cumbersome; however, it can be expressed as a function of the damping

for the isotropically loaded SC array D_I (eq. 7). For shear strains lower than $\gamma_t/10$, the ratio D_A/D_I is independent of the strain level, and it is closely approximated by the following linear relation:

$$[11] \quad \frac{D_A}{D_I} = 0.44 + 0.56SR$$

where SR is the stress ratio ($0.5 < SR < 2.5$). Hence, the damping of a shear wave propagating in a SC array will double when the stress ratio in the plane of polarization approaches $SR \approx 2.8$. However, the SC packing is "locked" and does not change with the stress ratio; this is not the case in soils.

Random packings

The low-strain, constant-fabric shear stiffness of statically isotropic packing under isotropic confining stress σ_o was computed by Chang et al. (1991) using Hertz and Mindlin contact theories:

$$[12] \quad G_{max} = \frac{(5 - 4\nu)}{5(2 - \nu)}\left[\frac{\sqrt{3}C_n}{\sqrt{2}\pi(1 - \nu)(1 + e)}\right]^{2/3}(G^2\sigma_o)^{1/3}$$

where ν and G are the Poisson's ratio and the shear modulus of the material of the particles, respectively, and e is the void ratio of the granular medium.

Chang et al. (1991) proposed a relationship for the low-strain Poisson's ratio for the packing (ν_{pack}) in terms of the Poisson's ratio for the particles (ν):

$$[13] \quad \nu_{pack} = \frac{\nu}{2(5 - 3\nu)}$$

Similar to the case of regular packings, the low-strain Poisson's ratio for the isotropic packing under isotropic stress conditions is smaller than Poisson's ratio of the particles (e.g., $\nu = 0.3$, $\nu_{pack} = 0.04$; see similar results in the review by Wang and Nur 1992).

A micromechanics-based close-form solution for wave attenuation in isotropic random packings would be governed by Mindlin's equation if the frictional contact loss is assumed, thus it will manifest stress and strain dependency, as observed in regular packings. No close-form solution was found for G, D, or ν of random packings subjected to anisotropic loading; a limited set of numerical results was presented by Chang et al. (1991).

Empirical relations for wave propagation parameters

Isotropic loading

Several investigators have proposed empirical expressions for G_{max} for soils under isotropic loading σ_o. These equations are of the following form:

$$[14] \quad G_{max} = Af(e)\sigma_o^b$$

hence,

$$[15] \quad V_s = A\sigma_o^{b/2}$$

where A and b are constants, and $f(e)$ is a function of void ratio (e.g., Hardin and Black 1966; Hardin and Drnevich 1972; Stokoe et al. 1985; Saxena et al. 1988). For example,

Fig. 1. Poisson's ratio of packing vs. Poisson's ratio of particles. Regular (body-centered cubic, BCC; cubic tetrahedral, CT; face-centered cubic, FCC) and random (Rnd) packings of monosize spheres (eqs. in Table 1 and eq. 13).

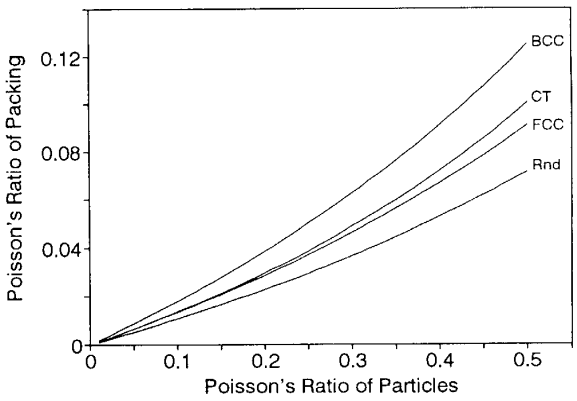

the empirical correction for void ratio proposed by Hardin and Drnevich (1972) is

$$[16] \quad f(e) = \frac{(2.97 - e)^2}{(1 + e)}$$

The parallelism between the empirical eq. 14 (after substitution of $f(e)$, eq. 16) and the micromechanics-based eq. 12 (after substitution of C_n, eq. 1) is remarkable. Hence, it appears that the constant A in eq. 14 is determined by the stiffness of the material of particles, at constant fabric.

There is a fundamental difference between the exponent b back-calculated by fitting eq. 14 to experimental data and the exponent of the stress in the G_{max} relation derived from micromechanical principles (eq. 12). In micromechanics analyses, b is a constant fabric parameter, that depends on the nature of contact stiffness (e.g., $b = 1/3$ for Hertzian contact, and $b = 1/2$ for cone-to-plane contact, Goddard (1990)). However, the measurement of b requires confining the medium at two different stress levels, causing fabric changes. Under isotropic stresses, fabric changes may produce significant variation in C_n, yet, changes in e may be imperceptible (compare predictions with eqs. 1, 2, and 3). Hence, the back-calculated exponent represents not only the nature of contact stiffness, but also the effect of changes in fabric.

An early empirical equation for damping in dry sands was proposed by Hardin (1965) and applies for the strain range $10^{-6} < \gamma < 10^{-4}$:

$$[17] \quad D = 0.985(\gamma^{0.2}\sigma_o^{-0.5})$$

The data used by Hardin (1965) to determine this equation were obtained by varying the confining pressure σ_o in kPa between $24 < \sigma_o < 144$ kPa, and the void ratio between $0.50 < e < 0.66$; the frequency was less than 600 Hz. This equation predicts that confinement and strain determine damping, similar to damping loss at Mindlin's contacts (eqs. 7 and 11).

Table 2. Relations for the hyperbolic model and the Ramberg-Osgood model (after Ishihara 1986).

Relation	Hyperbolic model	Ramberg-Osgood model
$\tau = f(\gamma)$ shear stress τ as function of shear strain γ; G_{max} is maximum shear modulus and τ_f is shear strength	$\tau = \dfrac{G_{max}\gamma}{1 + \dfrac{G_{max}\gamma}{\tau_f}}$	$\tau = \dfrac{G_{max}\gamma}{1 + \alpha_o\left\lvert\dfrac{\tau}{\tau_f}\right\rvert^{r-1}}$
$G_{sec} = f(\gamma)$ secant modulus G_{sec} as function of maximum shear strain γ_a; γ_r is a reference shear strain	$G_{sec} = \dfrac{G_{max}}{1 + \dfrac{\gamma_a}{\gamma_r}}$	$G_{sec} = \dfrac{G_{max}}{1 + \alpha_o\left\lvert\dfrac{G_{nor}\gamma_a}{\gamma_r}\right\rvert^{r-1}}$
$D = f(\gamma)$ damping ratio D as function of shear strain γ	$D = \dfrac{4}{\pi}\left(1 + \dfrac{1}{\dfrac{\gamma_a}{\gamma_r}}\right)\left[1 - \dfrac{1}{\dfrac{\gamma_a}{\gamma_r}}\ln\left(1 + \dfrac{\gamma_a}{\gamma_r}\right)\right]$	$D = \dfrac{2(r-1)}{\pi(r+1)}\alpha_o\dfrac{\left\lvert\dfrac{G_{nor}\gamma_a}{\gamma_r}\right\rvert^{r-1}}{1 + \alpha_o\left\lvert\dfrac{G_{nor}\gamma_a}{\gamma_r}\right\rvert^{r}}$
$D = f(G_{nor})$ damping ratio D as function of normalized shear modulus G_{nor}	$D = \dfrac{4}{\pi(1 - G_{nor})}\left[1 - \dfrac{G_{nor}}{1 - G_{nor}}\ln\left(\dfrac{1}{G_{nor}}\right)\right]$	$D = \dfrac{2(r-1)}{\pi(r+1)}[1 - G_{nor}]$

Note: Normalized shear modulus $G_{nor} = G_{sec}/G_{max}$, α_o, and r are constants.

Anisotropic loading

Two empirical relations have been suggested to relate the shear wave velocity V_s along principal directions with the state of stress in anisotropically loaded media. The stress in the direction of propagation σ_p and in the direction of particle motion σ_m are involved in both cases (Roesler 1979; Knox et al. 1982; Yu and Richart 1984; Santamarina and Fam 1995):

$$[18] \quad V_s = A\sigma_p^{\alpha}\sigma_m^{\beta}$$

where A, α, and β are constants. The alternative equation associates shear-wave velocity with the mean stress and deviatoric stress components on the polarization plane:

$$[19] \quad V_s = A\left(\frac{\sigma_p + \sigma_m}{2}\right)^{\zeta}\left(\frac{\sigma_p - \sigma_m}{2}\right)^{\psi}$$

where A, ζ, and ψ are constants. For isotropic confinement σ_o, both equations reduce to eq. 15, and the exponent ψ must be $\psi = 0$ (see also Yu and Richart 1984 for alternative forms of these equations that take explicitly into consideration the stress ratio). The authors are not aware of empirical equations to relate damping to anisotropic states of stress.

Corrections for strain level

Equations 18 and 19 are applicable for low-strain measurements ($\gamma < 10^{-5}$), i.e., G_{max} or V_{max}. Two simple models can be readily used to describe nonlinear behavior in particulate materials: the hyperbolic model and the Ramberg-Osgood model (Ishihara 1986). The stress–strain relationship and the variation of the shear modulus and damping with the strain level are summarized for each case in Table 2. Because the normalized modulus G/G_{max} and damping D are functions of the normalized strain γ/γ_r, a relationship between G/G_{max} and D can be derived for each model (also shown in Table 2).

Resonant column: anisotropic loading

The standard resonant column for isotropic loading (SBEL D1128) was modified for the application of deviatoric loads, keeping the fixed-free boundary conditions of the sample.

Axial compression (AC)

Deviatoric axial compression loading is applied by pulling the top cap downwards by means of a thin central cable (Fig. 2). Fixtures were designed to permit 3000 N gravity loading, which is equivalent to 750 kPa for the 7.1 cm diameter sample. A thin high-resistance steel cable (outside diameter, OD = 2.0 mm) extends vertically through the center of the sample and passes through the bottom plate of the confining cell. Pressures inside the sample and in the cell are isolated with O-ring seals. The effect of O-rings on the transmitted load was determined for different confining pressures. The force measured by a gaged stud inside the cell was compared against the external gravity load applied on the cable. For the range of confinements used in this study (30–600 kPa) the correction is small (±30 N).

Fig. 2. Axial compression modification to the resonant column device.

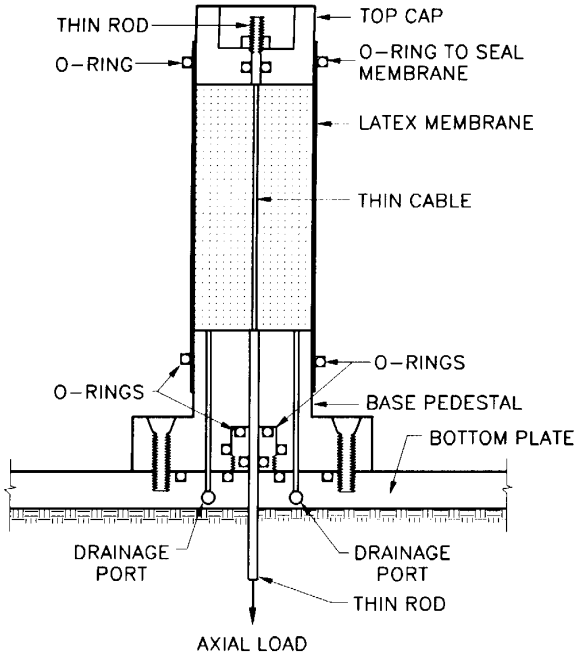

The dynamic effect of a thin rod passing through the sample was studied by Allen and Stokoe (1982). They found that the computed shear modulus of the soil becomes

$$[20] \quad G = V_s^2\left(\rho + \rho_r \frac{J_r}{J_s}\right) - G_r \frac{J_r}{J_s}$$

where J_s and ρ are the area polar moment of inertia and the mass density of the soil, respectively; J_r, ρ_r, G_r are the area polar moment of inertia, mass density, and shear modulus of the rod, respectively. A linear radial variation of shear strain was assumed in deriving eq. 20. The evaluation of this expression for typical parameters shows that the effect of the thin cable is negligible in the computation of the shear modulus of the soil. Allen and Stokoe (1982) experimentally verified that the influence of the rod was negligible on damping as well.

Axial extension (AE)

Deviatoric axial extension loading is imposed in a similar manner: the top cap is pulled upwards by means of a thin central cable (Fig. 3). The cable, which has the same mechanical characteristics as the one used in axial compression, is rigidly attached to the top cap. An internally gaged stud (Strainsert ST-FB) acts as load cell, and it is mounted in series with the cable. The stud extension passes through the top plate of the pressure cell and is pulled with a simple screw mechanism mounted on a spring with constant k = 270 N/cm. An O-ring seal is used to isolate the cell pressure. The gaged stud remains inside the cell, thus no load correction is needed.

Fig. 3. Axial extension modification to the resonant column device.

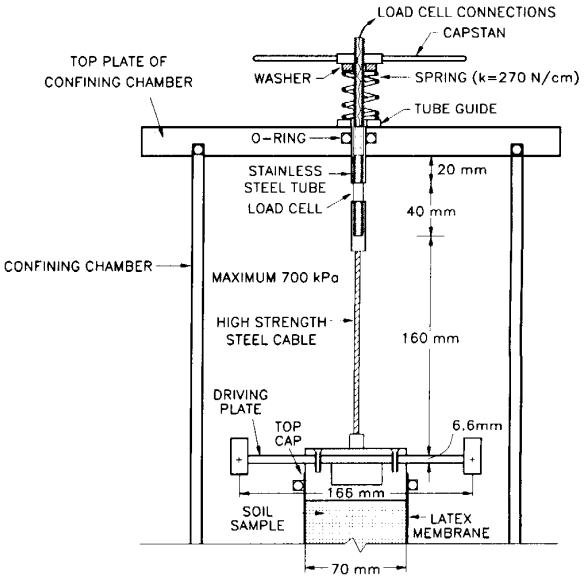

It can be shown that for this installation, the computed shear modulus of the soil becomes

$$[21] \quad G = V_s^2\left(\rho + \rho_r \frac{J_r L_s}{J_s L_r}\right) - G_r \frac{J_r L_s}{J_s L_r}$$

where L_s and L_r are the lengths the sample and of the thin rod, respectively. For L_r greater than L_s (our case), the effect of the thin cable in AE is smaller than in AC. The influence of the axial extension modification on resonant frequency and damping was experimentally studied using a calibrated aluminum probe. Results are summarized in Fig. 4. It can be concluded that for frequencies greater than 30 Hz the change in attenuation due to the thin cable is negligible and there is no significant effect on resonant frequency.

Calibration: driving system

The standard procedure for calibration with metal specimens was used. The mass polar moment of inertia of the driving system was recalibrated whenever changes were made, e.g., the connector added for axial extension testing. Calibration was performed for different AE tensile forces. The average computed stiffness of the aluminum specimen was very close to the value computed for the calibration without the AE fixtures, differences less than 1%. For damping, differences were also small, less than 3%.

Experimental studies

Tests with the resonant column were designed to experimentally study (1) the effect of anisotropic states of stress on wave propagation parameters, and (2) the relationship among damping, states of stress, and maximum shear strain under anisotropic states of stress. These studies were conducted using band-limited random noise excitation. Results

Fig. 4. Transfer function broad-band random noise, transfer function narrow-band random noise, and coherence for a calibration specimen: (*a*) without axial extension modification $D = 0.035$, $f_0 = 19.50$ Hz; (*b*) with axial extension modification $D = 0.034$, $f_0 = 19.22$ Hz (where f_0 is the natural frequency of the system).

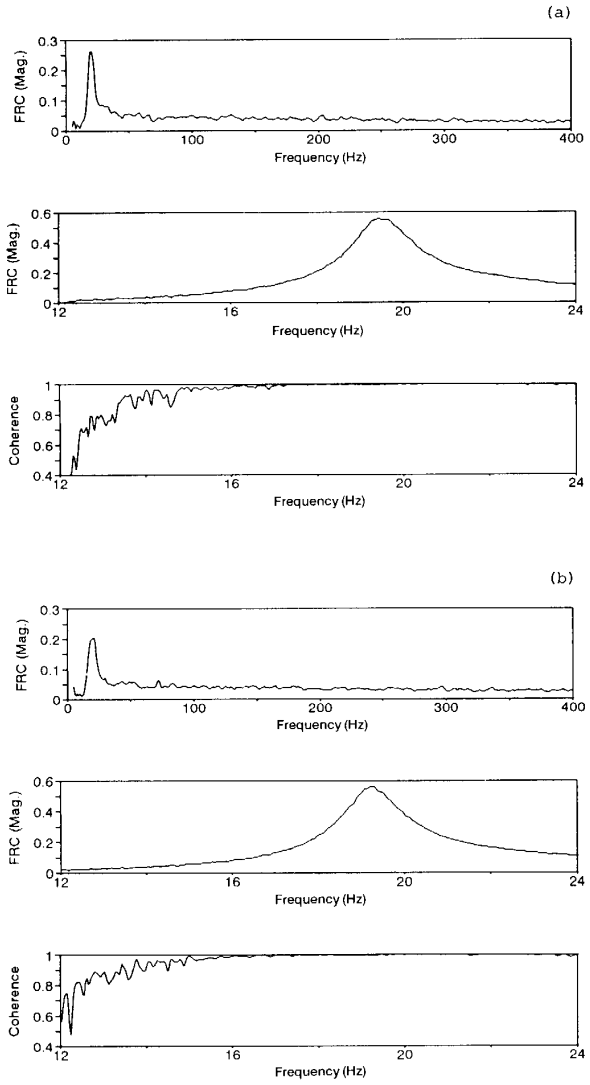

presented next include typical data for isotropic, axial extension, and axial compression loading.

Sample preparation: load history

A uniform, hard-grained sand was used in this study (Barco sand 32, $D_{50} = 0.44$ mm, $e_{max} = 0.73$, $e_{min} = 0.56$, $C_{u_3} = 1.5$, $C_c = 0.96$, SiO_2 content = 99.6%, and $G_s = 2.65$ g/cm^3). Samples were prepared by the dry pluviation technique from a constant falling height ($e \approx 0.60$, $D_r \approx 76\%$; sample length $L = 0.13$ m, diameter $d = 7.1$ cm). Once the upper platen was set in place, a vacuum was applied to hold the sample and the split mold was removed. Then, connections

Fig. 5. Stress–strain curves for dry sand (L, loading; U, unloading; I, isotropic): (*a*) axial extension (AE) test and (*b*) axial compression (AC) test.

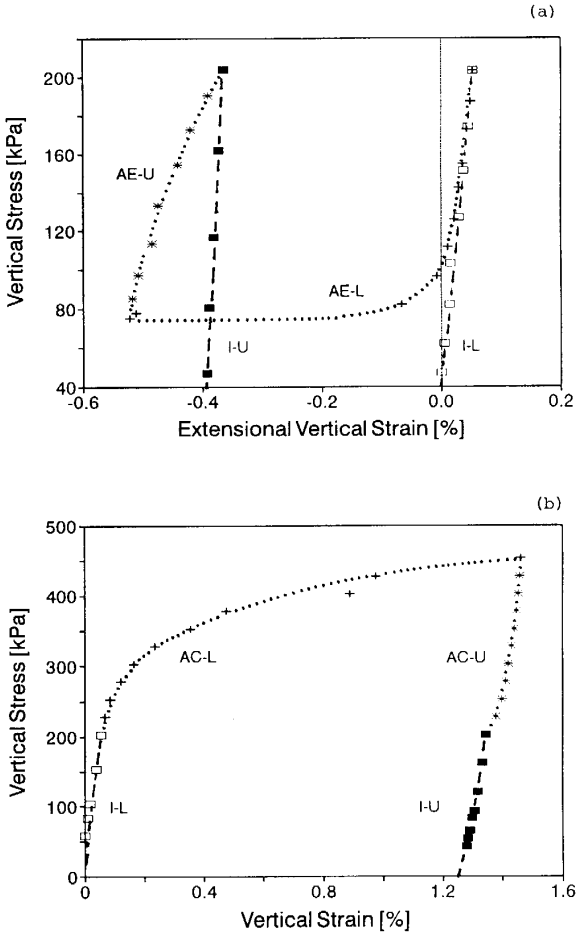

for the driving plate, linear varying displacement transducer (LVDT), and accelerometer were made, and the chamber was assembled. The sample vacuum was gradually released while increasing the cell pressure, until an effective confinement $\sigma_0 = 35$ kPa. Isotropic loading (IL) was applied to all samples tested in this study, increasing the confining pressure from 35 to 200 kPa. The additional loading history imposed on different samples included axial compression and axial extension. The stress–strain behavior for the two similar samples subjected to AE and AC is presented in Fig. 5. The void ratio was almost constant in all tests. Each load increment was maintained until all microseismic events had ended (10–30 min). Then, narrow-band random noise excitation with averaging was used to measure wave propagation parameters of samples.

Isotropic loading (IL)

Confinement was increased isotropically from 35 to 200 kPa, followed by a predefined cycle of deviatoric loading. The

Fig. 6. Variation in low-strain wave parameters during isotropic loading I-L and unloading I-U: (*a*) shear wave velocity and (*b*) damping.

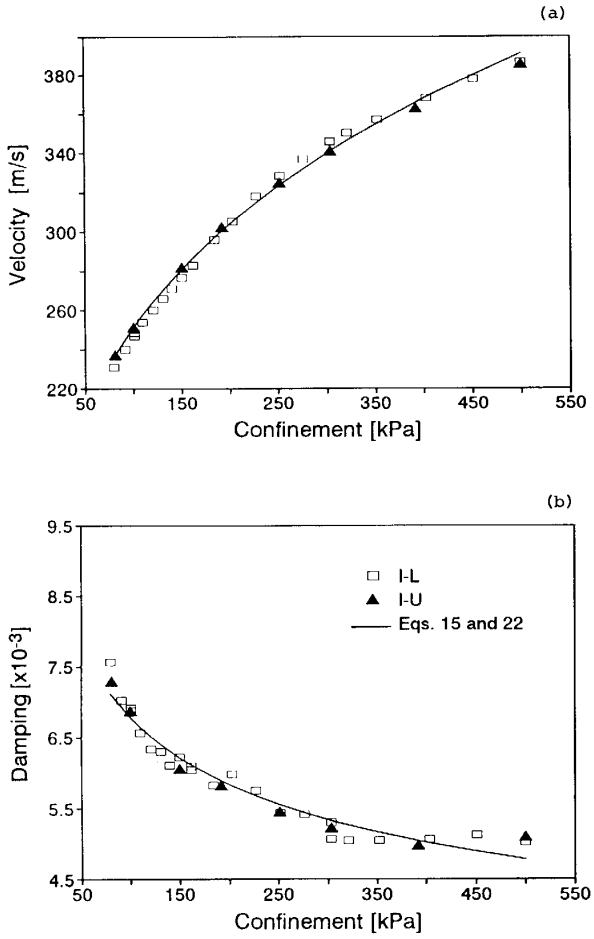

Fig. 7. Variation in low-strain wave propagation parameters for axial extension (AE) loading and unloading: (*a*) shear wave velocity and (*b*) damping.

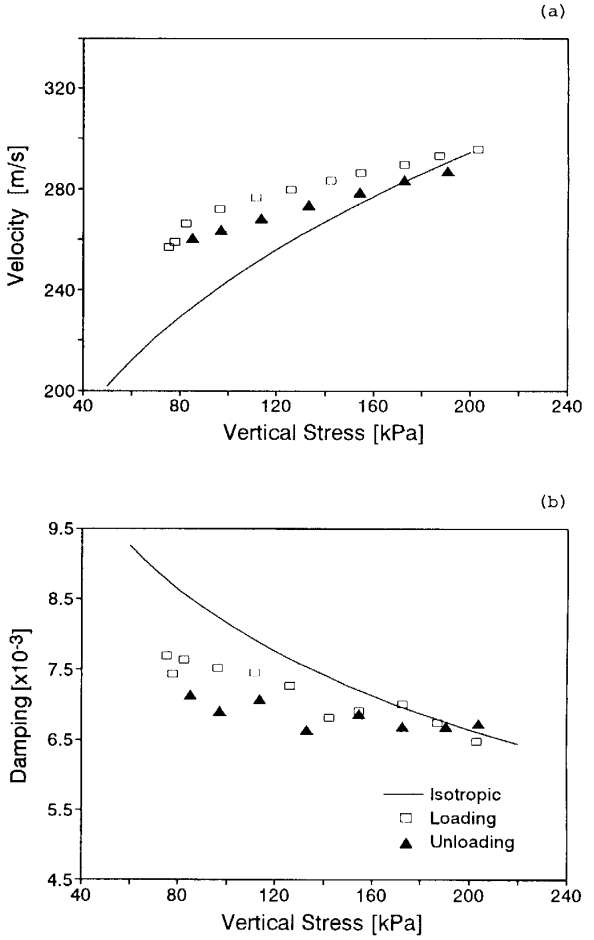

maximum axial strain reached during IL was $\varepsilon_z = 0.05\%$ in both AE and AC samples. The variations of velocity and damping with stress for IL are shown in Fig. 6.

Axial extension (AE)

Axial extension loading was imposed on sample AE after isotropic loading to $\sigma_0 = 200$ kPa. The stress–strain curve shows the nonelastic deformation induced upon loading (Fig. 5*a*), leaving a residual strain $\varepsilon_r = 0.4\%$. The maximum quasistatic axial strain during AE was one order of magnitude higher than the strain reached during isotropic loading.

Figure 7*a* shows the change in velocity V_s due to changes in the vertical stress. A reduction in velocity is observed during AE unloading, ending with a smaller value than at the initial isotropic condition; while the state of stress is identical, the change in velocity reflects residual fabric changes during deviatoric loading. Changes in damping are proportionally larger than changes in velocity. However, results show higher variability in damping than in velocity measurements.

Axial compression (AC)

Axial compression was conducted on sample AC, after isotropic loading to $\sigma_0 = 200$ kPa. Figure 5*b* shows the stress–strain plot; the residual deformation $\varepsilon_r = 1.2\%$ was three times greater than in AE (the maximum stress ratio was approximately the same). Figure 8*a* shows the evolution of velocity during loading and unloading; there are no residual effects due to fabric changes imposed during deviatoric loading. Wave velocity increased almost linearly with vertical stress, and at a lower rate than during isotropic loading. The same observations apply to damping (Fig. 8*b*).

Analyses and discussion

Velocity–stress and damping–stress relations (low strain)

The change in low-strain propagation velocity V_s with the increase in isotropic stress (Fig. 6*a*) was fitted with eq. 15 by linear regression analysis in log–log scale and verified by a nonlinear least-squares fitting algorithm (Table 3).

Table 3. Velocity–stress regression parameters.

Equation	Parameter	Related stress	Axial extension	Axial compression
[18]	α	σ_p	0.12	0.10
	β	σ_m	0.16	0.17
	$\alpha + \beta$	—	0.28	0.27
[19]	ζ	σ_{mean}	0.28	0.28
	ψ	$\sigma_{deviatoric}$	0.00	−0.01
	$\zeta + \psi$	—	0.28	0.27
[15]	$b/2$	σ_o	0.27	0.27

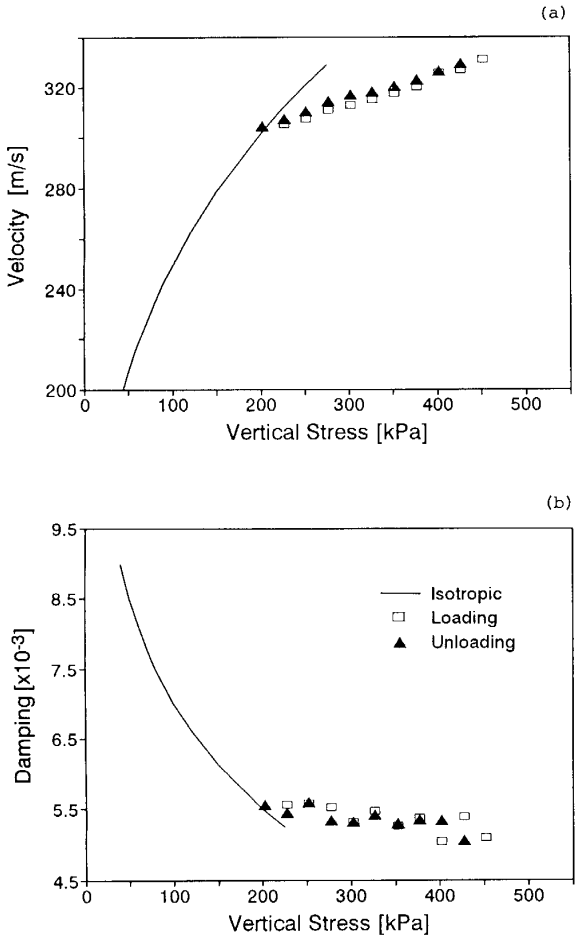

Fig. 8. Variation in low-strain wave propagation parameters for axial compression (AC) loading and unloading: (*a*) shear wave velocity and (*b*) damping.

The back-calculated velocity–stress exponent $b/2 = 0.27$ is in agreement with published data (e.g., Hardin and Richart 1963). The velocity–stress trend during AE and AC loading and unloading was fitted using eq. 18 (Table 3). The value of $\alpha + \beta$ is in agreement with the exponent measured under isotropic loading $b/2$. Back-calculated values for α and β imply that the stress in the direction of particle motion has a stronger influence on shear wave velocity than the stress in the direction of wave propagation (for comparison, see results in Viggiani and Atkinson 1995; Fam and Santamarina 1996, Stokoe et al. 1985). It follows from eq. 10 that the sensitivity of the body-centered cubic (BCC) shear stiffness to σ_m is also higher than to σ_p.

The same regression procedure was used to test the predictability of eq. 19. Values of ζ and ψ are listed in Table 3. The coefficient ζ is very similar to the isotropic exponent $b/2$. The value of ψ is close to zero even when isotropic data is not considered in the regression analysis; thus, shear wave velocity is mainly governed by the mean state of stress in the plane of polarization, at least within the stress ratios imposed in this study (Allen and Stokoe (1982) found that S-wave velocity in soils subjected to anisotropic loading were well described by either eq. 18 or eq. 19; Yu and Richart 1984 found that increasing the stress ratio decreases G_{max}, however, the reduction is not significant for stress ratios less than 2 or 3).

Wave velocity in anisotropic media is often modeled as elliptical or piece-wise elliptical (Helbig 1994). In the special case of weakly cross-anisotropy, the polar variation of V is expressed as a fourth-order Fourier series (only even terms; Crampin 1977). This is the same form of equations that are used to capture the polar anisotropy in micromechanical properties, as discussed previously. While it is tempting to conclude on the inherent link between these equations, values of ζ and ψ support the simpler relationship of V_s with the mean stress in the polarization plane. This is not the case with compressional propagation: experimental evidence shows that V_p depends on the stress in the direction of propagation (Kopperman et al. 1982; Hoque et al. 1995).

Observed trends in shear wave velocity during AE and AC loading are very similar to the predicted behavior for regular cubic packings at constant fabric (eq. 10). Figure 9*a* shows the change in shear wave velocity computed with eqs. 9 and 10 for a quartz sand (SC and BCC packings; $\nu = 0.15$, $G = 33$ GPa, mass density $\rho = 1.66$ kN·s^2/m^4). The representative velocity–stress exponent for BCC is 0.08 during AC loading (compare with $\alpha = 0.10$, Table 3) and 0.06 during AE (compare with $\alpha = 0.12$, Table 3).

Fig. 9. Variation in low-strain wave propagation parameters for regular packings subjected to isotropic and anisotropic loading (IL, AL) under constant fabric conditions: (*a*) shear wave velocity for SC eq. 9 and BCC eq. 10, (*b*) damping for SC eqs. 7 and 11.

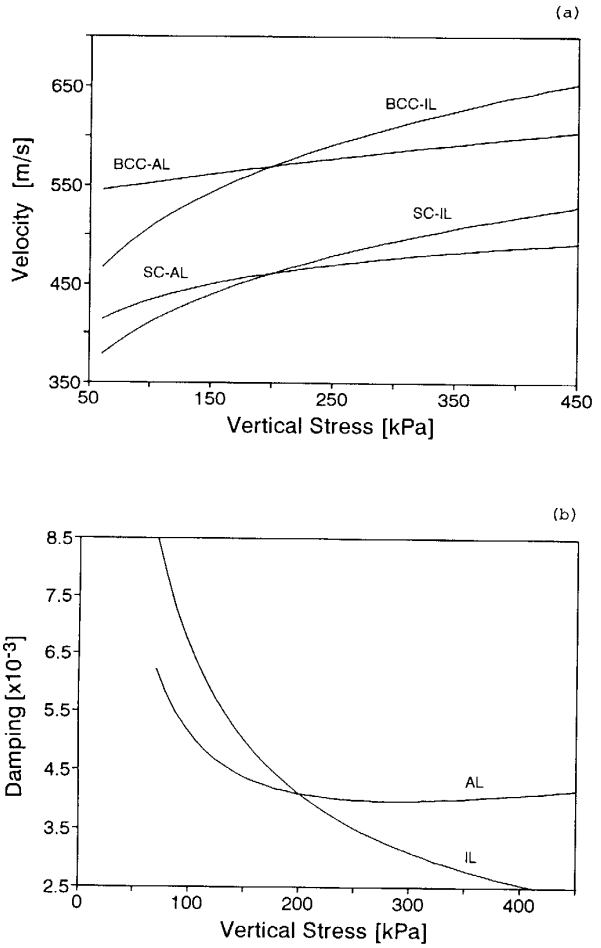

Fig. 10. Variation of wave propagation parameters with strain level and isotropic confinement. Measured data and fitted hyperbolic model trends: (*a*) shear wave velocity and (*b*) damping (modified hyperbolic model).

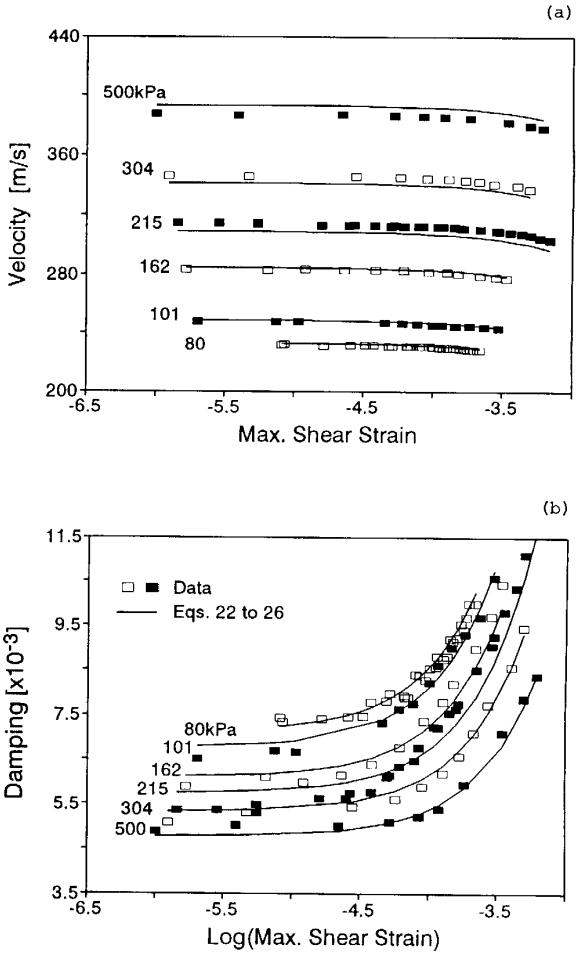

The variation of the low-strain damping D_{min} with isotropic loading (Fig. 6*b*) was fitted with a power relation, as suggested by micromechanical analyses (eq. 7 (see text)) and empirical observations (eq. 17):

$$D_{min} = 0.019\sigma_o^{-0.22} \quad [22]$$

The exponent is −0.22, while an exponent −2/3 was theoretically predicted for SC and FCC arrays based on Mindlin frictional contact loss. If the damping–stress power relationship is fitted to data obtained at higher strain levels, the exponent increases, indicating a higher mobilization of interparticle friction.

The change in damping at constant radial stress but subjected to AE and AC is shown in Figs. 7*b* and 8*b*. The general trend is closely matched by the power relation in eq. 22 in terms of the mean stress in the polarization plane. For comparison, the change in damping based on eqs. 7 and 11 for a SC packing is plotted in Fig. 9*b* for a constant strain $\gamma = 10^{-5.0}$. The maximum shear strain during AE and AC tests had a relative small variation $10^{-5.3} < \gamma < 10^{-5.0}$. The measured trends show qualitative agreement with predictions based on a SC array. Damping changed little, while the ratio SR = σ_p/σ_m changed from SR = 1 to SR = 0.4 for AE and from SR = 1 to SR = 2.25 for AC, for a constant σ_m = 200 kPa.

Velocity–strain and damping–strain relations (isotropic: middle strain)

The effect of isotropic confinement and strain level on shear wave velocity and damping is summarized in Fig. 10. Measurements were made on a dense sample (e = 0.58, D_r = 90%) to reduce the effects of fabric changes during testing. Equations in Table 2 were used to fit velocity and damping data. Both hyperbolic and Ramberg-Osgood models predict that damping (D_{model}) tends to zero at low strains ($\gamma < 10^{-6}$). Note that equations derived on the basis of

Mindlin contact have the same limitations for low-strain damping, as they are also based on a hysteretic model. This is not observed in the experimental data (see even the early results by Gardner et al. 1964).

The strain-independent D_{min} (eq. 22) was added to the damping equations in Table 2 to represent the minimum damping of the system, thus

[23] $D_{soil} = D_{model} + D_{min}$

Figure 10 shows that the hyperbolic model for velocity and the modified hyperbolic model for damping adequately represent the dependence of velocity and damping on shear strain ($10^{-6} < \gamma < 10^{-3.5}$) and confinement (80 kPa < σ_o < 500 kPa). The global nonlinear regression analysis of the data for all stress and strain ranges shows that γ_r and D_{min} vary with σ_o. The regression of velocity gave the following expressions for V_{max} (m/s) and γ_r in terms of confinement σ_o (kPa):

[24] $V_{max} = 66.48\sigma_o^{0.29}$

[25] $\gamma_r = 0.0053 + 1.42 \times 10^{-5}\sigma_o$

For damping data, the regression for D_{min} was presented above (eq. 22); the regression for γ_r in terms of confinement σ_o (kPa):

[26] $\gamma_r = 0.011 + 4.97 \times 10^{-5}\sigma_o$

Damping has higher sensitivity to shear strain level than shear wave velocity, while velocity only changed 4%, damping changed 90% (Fig. 10). The comparison of eqs. 25 and 26 indicates that confinement has a stronger influence in the reference strain γ_r for damping than for velocity.

The strain-independent minimum damping D_{min} implies the presence of nonhysteretic loss mechanisms at low strain. This can be foreseen: for a sand with average grain size $D_{50} = 10^{-3}$ m, and assuming an average strain field $\gamma \approx 10^{-7}$, the center-to-center relative displacement between two adjacent particles is 1 Å (1 Å = 0.1 nm), which is at the atomic level. Thus, other attenuation mechanisms must play an important role in real soils at low strains, including chemical interaction of adsorbed layers at contacts (Spencer 1981; Bulau et al. 1984), wave scattering (Blair 1990), thermal relaxation (Kjartansson 1979), and other forms of energy coupling (e.g., mechano-electromagnetic, mechano-acoustic). Potential loss mechanisms must satisfy independence of strain and the inverse affect of confinement. Any single model fails in justifying all observed trends in attenuation at low strains.

Conclusions

Analytical solutions for wave propagation parameters in *regular and random* packings were compiled from the literature or derived as part of this study. The similitude between published empirical equations and theoretical equations derived from micromechanical analyses is striking.

A resonant-column device was modified to allow for the application of deviatoric loads in axial extension and axial compression, in order to study the effect of stress anisotropy on wave propagation. The fixed-free boundary condition of the sample was maintained.

Velocity and damping showed minor residual changes upon deviatoric loading and unloading (residual strains 0.4–1.2%). Fabric changes that occurred during these loading paths had low effect on either wave parameter.

The shear wave velocity during the anisotropic loading of round, hard-grained sand is governed by the mean stress on the polarization plane, with minimal effect of the deviatoric component for stress ratios less than 2–3. When the role of stress components is differentiated, the stress in the direction of particle motion emerges more dominant. Shear wave velocity in the tested soil behaves similar to the shear stiffness of a body-centered cubic packing under anisotropic state of stress. The hyperbolic model adequately reflects the variation of shear wave velocity with confinement and shear strain.

Attenuation is strongly correlated with the mean stress on the polarization plane and the level of shear strain. However, damping does not vanish at low strains, contrary to predictions based on hysteretic behavior. Hence, the hyperbolic model must be modified by adding a minimum value D_{min}, which is independent on strain, yet it is function of confinement. The exponent of the power relation between low strain damping and confinement is significantly lower than predicted by Mindlin's frictional contact law. These observations suggest that friction is not the prevailing loss mechanism at low strain ($\gamma < 0.1\gamma_r$). Yet, measured damping changes in soils during anisotropic loading show similar trends to the changes in damping of a SC array with Mindlin contact when subjected to the same stress path.

Acknowledgments

This research is part of a study on wave–geomedia interaction and applications. Support was provided by the Natural Sciences and Engineering Research Council of Canada (NSERC) and the University of Waterloo ID-Program. The authors are indebted to Dr. N. Yassir and Dr. F. Tatsuoka for thoughtful comments and suggestions.

References

Allen, J.C., and Stokoe, K.H. 1982. Development of resonant column apparatus with anisotropic loading. Civil Engineering Department, University of Texas at Austin, Tex., Report GR82-28.

Aloufi, M., and Santamarina, J.C. 1995. Low and high strain macrobehaviour of grain masses—the effect of particle eccentricity. American Society Agricultural Engineers, **38**(3): 887.

Blair, D.P. 1990. A direct comparison between vibrational resonance and pulse transmission data for assessment of seismic attenuation in rock. Geophysics, **55**: 51–60.

Bulau, J.R., Tittmann, B.R., Abdel-Gawad, M., and Salvado, C. 1984. The role of aqueous fluids in the internal friction of rock. Journal of Geophysical Research, **89**(B6): 4207–4212.

Cascante, G. 1996. Low strain measurements with mechanical waves in geomaterials—implications in geotomography. Ph.D. thesis, University of Waterloo, Waterloo, Ont.

Chang, C.S., Misra, A., and Sundaram, S.S. 1991. Properties of granular packings under low amplitude cyclic loading. Soil Dynamics and Earthquake Engineering, **10**(4): 201–211.

Chantawarangul, K. 1993. Numerical simulations of three-dimensional granular assemblies. Ph.D. thesis, University of Waterloo, Waterloo, Ont.

Crampin, S. 1977. A review of the effects of anisotropic layering on the propagation of seismic waves. Geophysical Journal of the Royal Astronomical Society, **49**: 9–27.

Deresiewicz, H. 1973. Bodies in contact with applications to granular media. *In* R.D. Mindlin and Applied Mechanics. *Edited by* G. Herrmann. Pergamon Press, New York.

Dobry, R., Ladd, R.S., Yokel, F.Y., Chung, R.M., and Powell, D. 1982. Prediction of pore water pressure buildup and liquefaction of sands during earthquakes by the cyclic strain method. U.S. Department of Commerce, National Bureau of Standards, Building Science Series 138.

Duffy, J., and Mindlin, R.D. 1957. Stress–strain relations of a granular medium. Journal of Applied Mechanics, **24**(4): 585–593.

Fam, M., and Santamarina, J.C. 1996. A study of consolidation using mechanical and electromagnetic waves. Géotechnique. In press.

Fayed, M.E., and Otten, L. 1984. Handbook of powder science and technology. Van Nostrand Reinhold, New York.

Field, W.G. 1963. Towards the statistical definition of granular mass. Proceedings, 4th Australian and New Zealand Conference on Soil Mechanics, pp. 143–148.

Fratta, D., and Santamarina, J.C. 1996. Waveguide device for multi-mode, wideband testing wave propagation in soils. Geotechnical Testing Journal. In press.

Gardner, G.H.F., Wyllie, M.R.J., Doschack, D.M. 1964. Effect of pressure and fluid saturation on the attenuation of elastic waves in sands. Journal of Petroleum Technology, pp. 189–198. [Reprinted in Seismic Wave Attenuation, Society of Exploration Geophysicists Geophysics Reprint Series. *Edited by* Toksöz, M.N., and Johnston, D.H. 1981. Tulsa, Okla.].

Goddard, J.D. 1990. Nonlinear elasticity and pressure-dependent wave speeds in granular media. Proceedings of the Royal Society of London, London, Series A, **430**: 105–131.

Hardin, B.O. 1965. The nature of damping in sands. Journal of the Soil Mechanics and Foundations Division, ASCE, **91**(SM1): 63–97.

Hardin, B.O., and Black, W.L. 1966. Sand stiffness under various triaxial stresses. Journal of Soil Mechanics and Foundation Engineering, ASCE, **92**: 27–42.

Hardin, B.O., and Drnevich, V.P. 1972. Shear modulus and damping in soils: measurements and parameter effects. Journal of Soil Mechanics and Foundation Engineering, ASCE, **98**: 603–624.

Hardin, B.O., and Richart, F.E., Jr. 1963. Elastic wave velocities in granular soils. Journal of the Soil Mechanics and Foundations Division, ASCE, **89**(SM1): 33–63.

Helbig, K. 1994. Foundations of anisotropy for exploration seismics. Elsevier Science, New York.

Hoque, E., Tatsuoka, F., Sato, T., and Kohata, Y. 1995. Inherent and stress-induced anisotropy in small stiffness of granular materials. *In* Earthquake geotechnical engineering. *Edited by* K. Ishihara. A.A. Balkema Publishers, Rotterdam, Netherlands.

Ishihara, K. 1986. Evaluation of soil properties for use in earthquake response analysis. *In* Geomechanical modeling in engineering practice. *Edited by* R. Dungar and J.A. Studer. A.A. Balkema Publishers, Rotterdam, Netherlands.

Kjartansson, E. 1979. Constant Q-wave propagation and attenuation. Journal of Geophysical Research, **84**: 4737–4748.

Knox, D.P., Stokoe, K.H., II, and Kopperman, S.E. 1982. Effect of state of stress on velocity of low-amplitude shear waves propagating along principal stress directions in dry sand. Civil Engineering Department, University of Texas at Austin, Tex., Report GR82-23.

Kopperman, S.E., Stokoe, K.H., II, and Konox, D.P. 1982. Effect of state of stress on velocity of low-amplitude compression waves propagating along principal stress directions in dry sand. Civil Engineering Department, University of Texas at Austin, Tex., Report GR82-22.

Petrakis, E., and Dobry, R. 1987. Micromechanical modeling of granular soil at small strain by arrays of elastic spheres. Department of Civil Engineering, Rensselaer Polytechnic Institute, Troy, N.Y., Report CE-87-02.

Roesler, S.K. 1979. Anisotropic shear modulus due to stress anisotropy. Journal of Geotechnical Engineering, ASCE, **105**(GT7): 871–880.

Rothenburg, L., and Bathurst, R.J. 1989. Analytical study of induced anisotropy in idealized granular material. Géotechnique, **39**(4): 601–614.

Santamarina, J.C., and Fam, M. 1995. Changes in dielectric permittivity and shear wave velocity during concentration diffusion. Canadian Geotechnical Journal, **32**: 647–659.

Saxena, S.K., Avramidis, A.S., and Reddy, K.R. 1988. Dynamic moduli and damping ratios for cemented sands at low strains. Canadian Geotechnical Journal, **25**: 353–368.

Smith, W.O., Foote, P.D., and Busang, P.F. 1929. Packing of homogeneous spheres. Physics Review, **34**(9): 1271–1274.

Spencer, J.W. 1981. Stress relaxations at low frequencies in fluid-saturated rocks: Attenuation and modulus dispersion. Journal of Geophysical Research, **86**: 1803–1812.

Stokoe, K.H., Lee, S.H., and Knox, D.P. 1985. Shear moduli measurements under true triaxial stresses. Proceedings, Advances in the Art of Testing Soils Under Cyclic Conditions. Geotechnical Engineering Division, American Society of Civil Engineering, Detroit, Michigan, pp. 166–185.

Viggiani, G., and Atkinson, J.H. 1995. Stiffness of fine-grained soils at very small strains. Géotechnique, **45**(2): 249–265.

Wang, Z., and Nur, A. 1992. Elastic wave velocities in porous media: A theoretical recipe. Seismic and Acoustic Velocities in Reservoir Rocks, Vol. 2, pp. 1–35.

Yu, P., and Richart, F.E. 1984. Stress ratio effects on shear modulus of dry sands. Journal of Geotechnical Engineering, ASCE, **110**(3): 331–345.

List of symbols

α, β, ζ, ψ	exponents in velocity–stress power relationships
α_o, r	constants in Ramber-Osgood model
ε	normal strain (ε_z, maximum axial strain; ε_r, residual strain)
γ	shear strain (γ_a, maximum in cycle; γ_r, reference strain; γ_t, threshold)
ρ	mass density (ρ_r, mass density of the rod)
σ_o	isotropic confinement
σ_p, σ_m	stresses in the direction of wave propagation and particle motion, respectively
τ	shear stress
ν	Poisson's ratio
b	exponent in the modulus–stress relationship (isotropic loading)
e	void ratio
f	friction coefficient
f_o	natural frequency of the system
A	constant
C_n	coordination number
C_c, C_u	coefficient of curvature and uniformity in grain size distribution, respectively
D	damping ratio (D_A, anisotropic; D_I, isotropic; D_{min}, minimum damping)

D_r	relative density
E	Young's modulus
E_{loss}	energy loss per cycle
E_{return}	energy returned per cycle (elastic energy)
J_s, J_r	Areal polar moment of inertia of specimen and rod, respectively
G	shear modulus (G_{sec}, secant; G_{max}, maximum; G_r, modulus of rod)
G_{nor}	normalized shear modulus = G_{sec}/G_{max}
L_s, L_r	length of specimen and rod, respectively
M	constrained modulus
R	radius of the specimen
SR	stress ratio = σ_p/σ_m
V	wave velocity (V_s, shear; V_p, compressional)